The Journal of Chemical Physics

Surfactants and cloud droplet activation: A systematic extension of Köhler theory based on analysis of droplet stability

Cite as: J. Chem. Phys. **154**, 024707 (2021); https://doi.org/10.1063/5.0031436
Submitted: 01 October 2020 . Accepted: 20 December 2020 . Published Online: 13 January 2021

Robert McGraw, and Jian Wang

The Journal of Chemical Physics ARTICLE scitation.org/journal/jcp

Surfactants and cloud droplet activation: A systematic extension of Köhler theory based on analysis of droplet stability

Cite as: J. Chem. Phys. 154, 024707 (2021); doi: 10.1063/5.0031436
Submitted: 1 October 2020 • Accepted: 20 December 2020 •
Published Online: 13 January 2021

Robert McGraw[a] and Jian Wang[b]

AFFILIATIONS

Environmental and Climate Science Department, Brookhaven National Laboratory, Upton, New York 11973, USA

[a]**Author to whom correspondence should be addressed:** rlm@bnl.gov
[b]**Present address:** Center for Aerosol Science and Engineering, Department of Energy, Environmental and Chemical Engineering, Washington University in Saint Louis, Saint Louis, MO 63130.

ABSTRACT

The activation of aerosol particles to form cloud droplets, a necessary first step in cloud formation, controls much of the impact that aerosols have on clouds and climate. Recently, there has been a surge of interest in extending the Köhler theory of cloud droplet activation to include surface active (typically organic) as well as water-soluble (typically inorganic) aerosol components, but a systematic framework for doing this has yet to be developed. Here, we apply a droplet stability analysis to this end. Ideal and Szyszkowski–Langmuir surfactant models are analyzed to demonstrate the new approach, but the underlying theoretical framework is fundamental and model free. A key finding is that superficial densities at the cloud activation threshold (Köhler maximum) are significantly sub-monolayer, with fractional coverage ranging from 69% to 85% for the organic compounds and mixtures studied. The result, significant for model inventories of cloud condensation nuclei, is a weakening of the surfactant effect relative to expectations based on bulk sample measurements. Analytical results are obtained for the loci of Köhler maxima and applied to aerosol mixtures containing an arbitrary number of water-soluble and surfactant components.

I. INTRODUCTION

By providing a thermodynamic basis for determining the threshold level of water vapor saturation under which an aerosol particle activates to form a cloud drop, the Köhler theory (Köhler, 1936; Pandis and Seinfeld, 1998; and Pruppacher and Klett, 2010) has become an essential tool for assessing aerosol impacts on clouds and climate. Droplet growth kinetics and meteorological conditions aside, lower saturation thresholds result in more particles able to activate and higher cloud drop number concentrations. The latter, in turn, affects cloud properties both through enhanced cloud brightening (Twomey, 1977) and warm cloud drizzle suppression (Albrecht, 1989; McGraw and Liu, 2003; McGraw and Liu, 2004). Recently, it has been suggested that the staged activation of ultrafine aerosol particles having diameters between 15 nm and 50 nm can intensify the cores of the tropical deep-cloud convective systems that produce copious precipitation and drive global-scale circulation (Rosenfeld *et al.*, 2008; Fan *et al.*, 2018).

Atmospheric aerosols come in a variety of particle sizes and compositions that influence their ability to serve as cloud condensation nuclei (CCN). Early applications of Köhler theory treated mainly water-soluble species that lower the vapor pressure of aqueous solution droplets through the Raoult effect. More recently, there has been a surge in the number of theoretical and modeling studies focusing on the role of surfactants on CCN enhancement (e.g., Ovadnevaite *et al.*, 2017), or lack thereof (e.g., Raatikainen and Laaksonen, 2011), as well as laboratory measurements (e.g., Bilde and Svenningsson, 2004; Ruehl *et al.*, 2012; and Bzdek *et al.*, 2020). Despite considerable progress [see Lin *et al.* (2018) for a recent review], a systematic approach to bring surfactants into the

original Köhler framework remains to be developed. The present study is directed toward this goal.

The present study builds on the early analysis (Gibbs, 1878) of the stability properties of a spherical phase (here a nascent cloud droplet) embedded in an unspecified parent phase (here a surrounding atmosphere containing various levels of supersaturated water vapor) of indefinite extent. The nascent cloud droplet contains one or more nonvolatile solute species, each capable of varying degrees of size- and composition-dependent partitioning between the solution and the surface phase. It is shown here that the droplet stability analysis, when adapted to the Köhler problem beginning in Sec. III, provides a unified treatment of nascent cloud droplets containing mixtures of both water-soluble and surfactant species in equilibrium with water vapor at a Köhler maximum. The theory behind the new method is developed in Secs. IV–VI and applied to nascent cloud droplets in the sections that follow. Connections to nucleation theory are explored in Sec. VII. Section VIII presents a discussion and summary of the key results.

II. LOCI OF KÖHLER MAXIMA—SOLUBLE PARTICLE CASE

The activation thresholds for soluble aerosol particles to form cloud droplets under the levels of water vapor supersaturation encountered in the atmosphere, typically less than one or at most a few percent, is generally well described by Köhler theory (Köhler, 1936; Pruppacher and Klett, 2010). For (mostly) soluble components present in the condensation nucleus, the defining Köhler equation takes the form (Pandis and Seinfeld, 1998; Sorjamaa *et al.*, 2004)

$$\ln S = \frac{A_0}{r} - \frac{B}{r^3}, \tag{2.1}$$

where $S = P_w/P_w^{eq}$ is the water vapor saturation ratio at vapor pressure P_w. S equals unity when P_w equals P_w^{eq}, the equilibrium vapor pressure over the bulk liquid water reference state. The first term on the right-hand side is the contribution from the Kelvin equation, which gives the vapor pressure over a spherical drop of radius r in the absence of solute,

$$\ln S_K(r) = \frac{A_0}{r}, \tag{2.2}$$

where

$$A_0 = \frac{2\gamma_0 v_1}{kT} \tag{2.3}$$

is the Kelvin radius. γ_0 and v_1 are surface tension and molecular volume of water, k is Boltzmann's constant, and T is temperature. The second term in Eq. (2.1) represents the contribution from the dissolved solute. The Köhler critical volume (droplet volume at maximum supersaturation) is typically hundreds of times larger than the dry particle volume, justifying the dilute solution approximation that gives this term its r^{-3} dependence,

$$\ln S_b(r) = -\frac{B}{r^3} \approx -x_2. \tag{2.4}$$

x_2 is the molecular (or molar) ratio of dissolved solute (component 2) to liquid water (component 1) present in the drop, n_2^b/n_1. In the absence of partitioning to the surface, n_2^b equals the total number of solute molecules n_2. S_b is the equilibrium vapor saturation ratio over a bulk solution having the composition of the drop. With this result, Eq. (2.1) becomes

$$\ln S = \frac{A_0}{r} - x_2, \tag{2.5}$$

also known as the Gibbs–Kelvin–Köhler (GKK) equation (Shchekin and Rusanov, 2008).

Two universal curves for soluble inorganics: Several geometric relations are exhibited in Fig. 1. First, it is evident from Eq. (2.1) that $\ln S$ assumes its maximum value, $\ln S_c$, at a critical radius r_c given by

$$r_c^2 = 3B/A_0 \tag{2.6}$$

for A_0 and B independent of radius.

There is a ready separation of the parameters A_0 and B at the critical size. Isolating A_0 gives

$$\ln S_c(r_c) = \frac{A_0}{r_c} - \frac{B}{r_c^3} = \frac{A_0}{r_c} - \frac{(BA_0/(3B))}{r_c} = \frac{2}{3}\frac{A_0}{r_c}. \tag{2.7}$$

The last equality shows that the locus of Köhler critical points follows a universal curve, for the dissolved solute effect, at 2/3 height of the Kelvin curve, independent of dry seed particle composition and size. This is the upper dashed curve in Fig. 1 separating the stable (left) and unstable (right) branches of the Köhler curve. The Kelvin curve is itself the locus of critical nuclei in homogeneous nucleation theory (Reiss and Koper, 1995).

A second universal curve, this for the locus of critical drop composition, x_{2c}, is obtained for the bulk solute contribution,

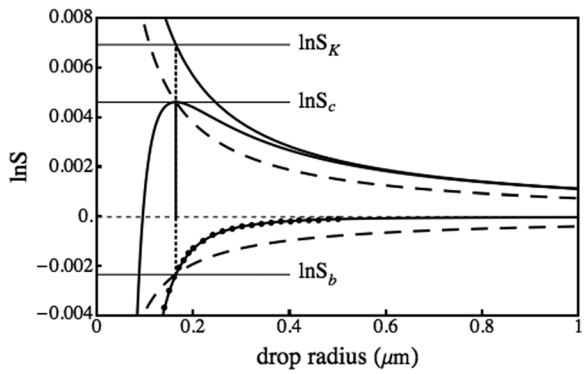

FIG. 1. Properties of the Köhler equation: solid curves top to bottom: Kelvin, full Köhler, and bulk solute terms of Eq. (2.1) for a NaCl dry seed radius of 20 nm. The bulk solute term was obtained from a fit of Eq. (2.4) to water activities calculated from the Pitzer model (Pitzer, 1973) (black dots). Vertical lines positioned at the Köhler maximum indicate various displacements described in the text [Eq. (2.8)]. Upper and lower dashed curves define the locus of Köhler maxima and the saturation ratio over bulk solution having the composition of the critical drop as functions of the critical droplet radius r_c.

$$\ln S_b(r_c) = -\frac{B}{r_c^3} = -x_{2c} = -\frac{1}{3}\frac{A_0}{r_c} = -\frac{1}{3}\ln S_K(r_c) = -\frac{1}{2}\ln S_c(r_c). \tag{2.8}$$

The third equality uses Eq. (2.6) to eliminate B. Equation (2.8) generates the lower dashed curve of Fig. 1. It is interesting that knowledge of the water activity alone, $a_W \approx S_b$, is sufficient to determine the critical radius, solute activity, and Köhler maximum. A related situation is found in observations that the freezing and nucleation thresholds for ice formation, also from dilute aqueous solutions, are largely controlled by water activity (Koop *et al.*, 2000). Both cases derive from dilute solution thermodynamics and reflect the dominating importance of water activity in this regime.

Connections to the κ–Köhler model: Petters and Kreidenweis (2007) defined a hygroscopicity parameter κ through its effect on water activity,

$$\frac{1}{a_w} = 1 + \kappa\frac{V_s}{V_w}. \tag{2.9}$$

V_s and V_w are the volumes of dry particle seed and water in the droplet. For the dilute solutions under consideration, one has to good approximation

$$\ln a_w = -\ln\left(1 + \kappa\frac{V_s}{V_w}\right) \approx -\kappa\frac{V_s}{V_w} \approx -\kappa\frac{r_{dry}^3}{r^3} = -x_2 = \ln S_b. \tag{2.10}$$

Comparing with the first equality of Eq. (2.8) gives

$$B \approx \kappa r_{dry}^3, \tag{2.11}$$

where r_{dry} is the volume-equivalent dry particle radius. Using B from the fit to the Pitzer model (c.f. Fig. 1) yields a kappa value for NaCl, κ_2, of 1.25, in good agreement with the reported mean CCN-derived value of 1.28 (Petters and Kreidenweis, 2007). The approximate equality in Eq. (2.11) refers to the dilute solution limit, in which case combining Eqs. (2.6) and (2.11) gives

$$r_c^2 = \frac{3B}{A_0} = \frac{3\kappa}{A_0}r_{dry}^3 = \frac{3kT\kappa}{2\nu_1\gamma_0}r_{dry}^3 \tag{2.12}$$

and the proportionality $r_c^2 \propto r_{dry}^3$ (Petters and Kreidenweis, 2007; Lewis, 2008). The next-to-last equality in Eq. (2.10) makes use of Eq. (2.11) to expand the definition of x_2 from the molecular ratio, n_2^b/n_1, to $x_2 = \kappa r_{dry}^3/r^3$, which reduces to the molecular ratio for a dilute, non-dissociating solute, $\kappa = \kappa_{ideal} = \nu_1/\nu_2$, where ν_2 is the molecular volume of the solute in the dry particle. The expanded definition brings in solute non-ideality and other useful properties of κ, not the least of which is its tabulation for many atmospheric compounds of relevance to cloud droplet activation.

III. EQUIVALENCE BETWEEN THE KÖHLER AND GIBBS DROPLET STABILITY CONDITIONS

In Sec. II, it was mentioned that the locus of Köhler maxima separates each Köhler curve into stable and unstable branches according to the sign of $d\ln S/dr$. By stable (unstable), we refer to the tendency for a small droplet, located initially along the Köhler curve, to return to (depart from) its original state after a small disturbance. The condition for stability, henceforth the Köhler stability condition (KSC), is

$$d\ln S/dr > 0 \tag{3.1}$$

with the direction of inequality reversed for instability and equality ($d\ln S/dr = 0$) at the Köhler maximum. Inequality (3.1) is satisfied for droplets smaller (more concentrated) than those of critical size and reversed for larger (less concentrated) ones, corresponding to the stable and unstable branches of the Köhler curve (Reiss and Koper, 1995).

Gibbs, in his treatment of the stability of a spherical phase embedded in an unspecified background phase of indefinite extent, started with a mechanical condition for stability based on the pressure difference, $\Delta P = 2\gamma/r$, across the interfacial boundary (Gibbs, 1878),

$$\left(r\frac{d\Delta P}{dr} - 2\frac{d\gamma}{dr}\right) = \left(r\frac{d\Delta P}{d\mu_2} - 2\frac{d\gamma}{d\mu_2}\right)\frac{d\mu_2}{dr} < -\Delta P. \tag{3.2}$$

The introduction of chemical potential in the middle expression is a pivotal step that begins transformation of the mechanical stability problem into a molecular one. Further reductions using the Gibbs adsorption equation

$$\frac{d\gamma}{d\mu_2} = -\frac{n_2^s}{4\pi r^2} = -\Gamma_2, \tag{3.3}$$

where Γ_2 is the superficial density, and its analog for the change in pressure,

$$\frac{d\Delta P}{d\mu_2} = \frac{n_2^b}{V} \approx \frac{n_2^b}{n_1 v_1} = \frac{x_2}{v_1}, \tag{3.4}$$

where V is the droplet volume, complete the transformation

$$\left(r\frac{x_2}{v_1} + 2\Gamma_2\right)\frac{d\mu_2}{dr} < -\Delta P, \tag{3.5}$$

henceforth the Gibbs stability condition (GSC). The approximate equality in Eq. (3.4) reflects the dilute solution approximation.

Application of the Gibbs analysis to the Köhler problem requires first demonstrating that the two conditions (KSC and GSC) are equivalent. This can be done by transforming inequalities (3.1) and (3.5) into one another as follows: On differentiation of the Gibbs–Kelvin–Köhler equation [Eq. (2.5)] and rearranging terms, the KSC becomes

$$rkT\frac{d}{dr}(x_2/v_1) - 2\frac{d\gamma}{dr} < -\Delta P. \tag{3.6}$$

Next, the chemical potential is introduced as in (3.2),

$$\left(rkT\frac{d}{d\mu_2}(x_2/v_1) - 2\frac{d\gamma}{d\mu_2}\right)\frac{d\mu_2}{dr} = \left(r\frac{x_2}{v_1} + 2\Gamma_2\right)\frac{d\mu_2}{dr} < -\Delta P, \quad (3.7)$$

where the equality, showing final reduction to the GSC, follows (3.3) and $\mu_2 = kT \ln x_2$. The two stability conditions are indeed equivalent.

Conditions at the Köhler maximum may be obtained analytically by equating two independent expressions for $d\mu_2/dr$: The first, valid only at the Köhler maximum, is obtained by simply solving (3.7) in the equality limit,

$$\frac{d\mu_2}{dr} = -\Delta P/\left(r\frac{x_2}{v_1} + 2\Gamma_2\right) = -2\gamma/\left(r^2\frac{x_2}{v_1} + 2r\Gamma_2\right). \quad (3.8)$$

The second, valid at any droplet radius, is obtained from the conservation condition, $n_2^b + n_2^s = n_2$. In the expanded form,

$$\frac{4\pi r^3}{3}\left(\frac{x_2}{v_1}\right) + 4\pi r^2\Gamma_2 = n_2.$$

Differentiation holding n_2 constant gives

$$\left(r^2\frac{x_2}{v_1} + 2r\Gamma_2\right)dr + \frac{1}{3}r^3 d\left(\frac{x_2}{v_1}\right) + r^2 d\Gamma_2 = 0,$$

which, as x_2 and Γ_2 are functions of μ_2, becomes

$$\left(r\frac{x_2}{v_1} + 2\Gamma_2\right)dr + \left(\frac{r^2}{3}\frac{d(x_2/v_1)}{d\mu_2} + r\frac{d\Gamma_2}{d\mu_2}\right)d\mu_2 = 0,$$

yielding for the second expression

$$\frac{d\mu_2}{dr} = -\frac{\left(r\frac{x_2}{v_1} + 2\Gamma_2\right)}{\frac{r^2}{3}\frac{d(x_2/v_1)}{d\mu_2} + r\frac{d\Gamma_2}{d\mu_2}}. \quad (3.9)$$

Substituting into (3.5) gives the general stability condition for a single component solute partitioned between the surface and the volume of the droplet,

$$\frac{\left(r\frac{x_2}{v_1} + 2\Gamma_2\right)^2}{\frac{r^2}{3}\frac{d(x_2/v_1)}{d\mu_2} + r\frac{d\Gamma_2}{d\mu_2}} > \Delta P. \quad (3.10)$$

Equations (3.9) and (3.10) (equality case) are general expressions that may be adapted to any physically consistent model of the solution and surface phases. The bulk solution and surfactant limiting cases of (3.10) are especially simple and insightful to the analysis of the Köhler problem.

In the surfactant limit, $x_2 \to 0$, (3.10) reduces to the condition

$$\frac{(2\Gamma_2)^2}{r\frac{d\Gamma_2}{d\mu_2}} = -\frac{4\Gamma_2\frac{d\gamma}{d\mu_2}}{r\frac{d\Gamma_2}{d\mu_2}} = -\frac{4\Gamma_2}{r}\frac{d\gamma}{d\Gamma_2} > \Delta P = \frac{2\gamma}{r}, \quad (3.11)$$

where in the first equality, the adsorption equation (3.3) has been used to eliminate one of the Γ_2's. Rearranging the inequality gives the following elegantly simple condition for stability:

$$\frac{\Gamma_2}{\gamma}\frac{d\gamma}{d\Gamma_2} < -\frac{1}{2}. \quad (3.12)$$

The left-hand side equals $-1/2$ at the Köhler maximum and exceeds $-1/2$ in the unstable regime. (3.12) is a general result that is applied in Sec. IV to the Köhler problem using two different surfactant models.

Similar reduction of the general stability formula for the bulk limit, $\Gamma_2 \to 0$, gives the complementary result for this case. By inspection, (3.10) reduces to

$$\frac{\left(r\frac{x_2}{v_1}\right)^2}{\frac{r^2}{3}\frac{d(x_2/v_1)}{d\mu_2}} = \frac{(x_2/v_1)\left(\frac{d\Delta P}{d\mu_2}\right)}{\frac{1}{3}\frac{d(x_2/v_1)}{d\mu_2}} > \Delta P, \quad (3.13)$$

where now (3.4) has been used to eliminate one of the concentration factors in the numerator. Finally, on dividing through by ΔP and rearranging terms,

$$\frac{x_2/v_1}{\Delta P}\frac{d\Delta P}{d(x_2/v_1)} > \frac{1}{3}. \quad (3.14)$$

Gibbs extended the GSC to multiple solute species (in the case of present interest component 1 being water),

$$\left(r\frac{x_2}{v_1} + 2\Gamma_2\right)\frac{d\mu_2}{dr} + \left(r\frac{x_3}{v_1} + 2\Gamma_3\right)\frac{d\mu_3}{dr} + \cdots < -\Delta P. \quad (3.15)$$

Each derivative is evaluated using its own molecular conservation condition with the chemical potentials of the other solutes present held constant. (3.15) is applied in Sec. VI to obtain the loci of Köhler maxima for mixtures of two or more solutes in terms of their relative abundances in the dry aerosol particle seed.

IV. ANALYSIS OF DROP STABILITY WITH APPLICATION TO THE KÖHLER PROBLEM

The Gibbs analysis, as modified for the Köhler problem in Sec. III, is used here to develop a systematic formulation of the Köhler theory that treats contributions from the bulk solution and surface layer in a more or less symmetric fashion while yielding analytic, largely model independent, expressions for critical droplet properties. To this end, we apply stability analysis, initially to the solution phase (Sec. IV A), so as to recover the results of Sec. II from a broader perspective that is applicable as well to the surface (Sec. IV B).

A. Bulk limit

The bulk limit stability condition (3.14), taken in the equality limit, is satisfied at the neutral equilibrium condition corresponding to the maximum of the Köhler curve. Of interest here is the

saturation ratio, which peaks at the Köhler maximum. ΔP is the Laplace pressure inside the droplet relative to that of the surrounding vapor. The two quantities are related [c.f. Eqs. (2.3) and (2.5)] through the identity

$$kT(\ln S + x_2) = v_1 \Delta P, \tag{4.1}$$

where in general $\Delta P = 2\gamma/r$, with surface tension $\gamma = \gamma_0$ in the bulk limit. Equation (4.1) brings in the saturation ratio and a more convenient expression of (3.14) for addressing the Köhler problem,

$$\frac{x_2}{\ln S + x_2} \frac{d(\ln S + x_2)}{dx_2} > \frac{1}{3}.$$

At the Köhler maximum $\ln S = \ln S_c$, $d \ln S = 0$, and the derivative is unity. At equality,

$$\frac{x_{2c}}{\ln S_c + x_{2c}} = \frac{1}{3},$$

where the subscript "c" refers to conditions at the Köhler maximum. This yields the immediate result that $\ln S_c = 2x_{2c}$. From the equality $\ln S_c + x_{2c} = \ln S_K$ at any critical radius—the Kelvin (pure water) and solution droplets being under the same Laplace pressure at the same radius and same surface tension γ_0—one obtains the explicit solutions, $x_{2c} = \ln S_K/3$ and $\ln S_c = 2 \ln S_K/3$, thereby recovering the two universal curves of Sec. II.

B. Surfactant limit

The complementary inequality for stability in the surfactant limit, i.e., no appreciable solute effect, is given by (3.12),

$$\frac{kT\Gamma_2}{\gamma} \frac{d\gamma}{dkT\Gamma_2} < -\frac{1}{2}, \tag{4.2}$$

where each of the factors on the left-hand side of (3.12) has been made dimensionless by multiplying and dividing by kT. $\gamma(r)$ is the surface tension of the droplet, generally different from γ_0 and radius dependent, and $\Gamma(r)$ is the superficial density,

$$\Gamma_2(r) = n_2^s/(4\pi r^2). \tag{4.3}$$

n_2^s refers to the number of solute molecules present at the surface of the drop. In the strong surfactant limit, $n_2^s = n_2$.

Inequality (4.2) is valid for any physically consistent surfactant model, with the proviso that the droplet be large relative to the thickness of its interface. Only then, as Gibbs himself noted, will the mathematical "dividing surface" he invented sensibly coincide with the physical surface of discontinuity, making droplet radius, surface tension, and other quantities dependent on dividing surface placement for small clusters, physically well defined for larger droplets. The coincidence of dividing surfaces further implies that effects due to the intrinsic curvature on droplet surface tension can be neglected (Buff, 1952; Laaksonen *et al.*, 1999). Similar arguments show that surface excess quantities and physical surface concentrations are equivalent under such conditions (Bermúdez-Salguero and Gracia-Fadrique, 2015; Toribio *et al.*, 2018). This restriction is of no consequence for the critical-size droplets of Köhler theory where the interfacial thickness to droplet radius ratios is typically of order one percent.

To accommodate surfactants, the Köhler theory is extended to allow the lowering of surface tension from that of pure water. Allowing for radius dependence, Eq. (2.5) becomes

$$\ln S = \frac{A_0}{r} - \frac{2[\gamma_0 - \gamma(r)]v_1}{rkT} - x_2. \tag{4.4}$$

For $\gamma = \gamma_0$, the middle term vanishes and results from Sec. II are obtained.

Szyszkowski–Langmuir (SL) surfactant model: The Szyszkowski equation for surface tension has the form (Meissner and Michaels, 1949)

$$\gamma_0 - \gamma = kT\Gamma_m \ln(1 + Kx_2), \tag{4.5}$$

where x_2 is equated to the solute activity, with chemical potential $\mu_2 = kT \ln x_2$ in the dilute solution approximation. Differentiating with respect to $\ln x_2$ gives

$$\frac{d(\gamma_0 - \gamma)}{d \ln x_2} = -\frac{d\gamma}{d \ln x_2} = kT\Gamma_m \frac{Kx_2}{1 + Kx_2} = kT\Gamma_2 \tag{4.6}$$

and the Langmuir adsorption isotherm (Adamson and Gast, 2012)

$$\Gamma_2/\Gamma_m = \frac{Kx_2}{1 + Kx_2}. \tag{4.7}$$

The equality between the second and last terms of Eq. (4.6) follows the Gibbs adsorption equation [Eq. (3.3)]. The surface layer saturates at a superficial density Γ_m, interpreted as full monolayer coverage. K determines the extent of solute partitioning between surface and bulk. Combining the Szyszkowski and Langmuir forms, Eqs. (4.5) and (4.7), respectively, yields surface tension reduction in terms of superficial density,

$$\gamma_0 - \gamma = kT\Gamma_m \ln\left(\frac{1}{1 - \frac{\Gamma_2}{\Gamma_m}}\right), \tag{4.8}$$

and the dimensionless derivative,

$$\frac{d\gamma}{dkT\Gamma_2} = -\frac{1}{\left(1 - \frac{\Gamma_2}{\Gamma_m}\right)}. \tag{4.9}$$

Equations (4.8) and (4.9) contain all of the ingredients needed for the evaluation of droplet stability. Substitution into (4.2), equality case, gives

$$-\frac{1}{\left(1 - \frac{\Gamma_{2c}}{\Gamma_m}\right)} \times \frac{kT\Gamma_{2c}}{\gamma_0 - kT\Gamma_m \ln\left(\frac{1}{1 - \frac{\Gamma_{2c}}{\Gamma_m}}\right)} = -\left(\frac{\gamma_{\text{int}} - \gamma_c}{kT\Gamma_{2c}}\right)\left(\frac{kT\Gamma_{2c}}{\gamma_c}\right)$$
$$= -\left(\frac{\gamma_{\text{int}} - \gamma_c}{\gamma_c}\right) = -\frac{1}{2}, \tag{4.10}$$

where γ_{int} is the tangent intercept in the graphical construction introduced in Fig. 2. Equation (4.10) is readily solved for the critical superficial density and surface tension, Γ_{2c} and γ_c, respectively, given Γ_m and γ_0.

The first equality of Eq. (4.10) has a simple interpretation in terms of Fig. 2, which shows surface tension plotted as a function of superficial density from Eq. (4.8). The curve is independent of the partition coefficient K, which can easily vary orders of magnitude. From another perspective, all such curves having the same monolayer coverage but different partition coefficients project onto this one curve. Meissner and Michaels, in their study of the surface tensions of dilute aqueous solutions, grouped together some 25 aliphatic organic compounds covering a wide range of K, functional groups, and solubility, assigning the same monolayer coverage, $kT\Gamma_m = 12.99$, to each member of the group. The compounds included a number with alkyl chains that, depending on their orientation at the surface, might well exhibit similar monolayer densities. Using this monolayer value, and $\gamma_0 = 72.8$, the unique solution to Eq. (4.10) gives $\Gamma_{2c}/\Gamma_m = 0.689$, $kT\Gamma_{2c} = 8.955$, and surface tension at the Köhler maximum, $\gamma_c = 57.6\ erg/cm^2$.

With reference to the tangent construction of Fig. 2 and the last equality of 4.10, we have $\gamma_c = 2\gamma_{\text{int}}/3$ in the surfactant limit. As the coordinates, γ_c and Γ_c, are thereby fixed for a given solute at the Köhler maximum, their independence on seed particle size is implied. The constancy of γ_c, in turn, implies that the locus of Köhler maxima is again a constant fraction, in this case γ_c/γ_0, of the Kelvin curve,

$$\ln S_c = \frac{2\nu_1\gamma_c}{kTr_c} = \frac{\gamma_c}{\gamma_0}A_0/r_c = \frac{2}{3}\frac{\gamma_{\text{int}}}{\gamma_0}A_0/r_c. \tag{4.11}$$

Identification of the Köhler maximum is complete upon determination of r_c. From (4.2), expressed as an equality, and (4.3) for the superficial density, we obtain

$$r_c^2 = \frac{kTn_2}{4\pi\, kT\Gamma_c} = 2\left(\frac{1}{1-\frac{\Gamma_c}{\Gamma_m}}\right)\frac{kTn_2}{4\pi\gamma_c}. \tag{4.12}$$

The constancy of Γ_c and γ_c in (4.12) implies the same proportionality, $r_c^2 \propto n_2 \propto r_{dry}^3$, as was previously found in the bulk limit [Eq. (2.12)]. The quantity in parentheses is the magnitude of the tangent slope, evaluated at the Köhler maximum. Together, Eqs. (4.11) and (4.12) give an analytic determination of the saturation ratio at the activation threshold for any given set of SL parameters, K and Γ_m.

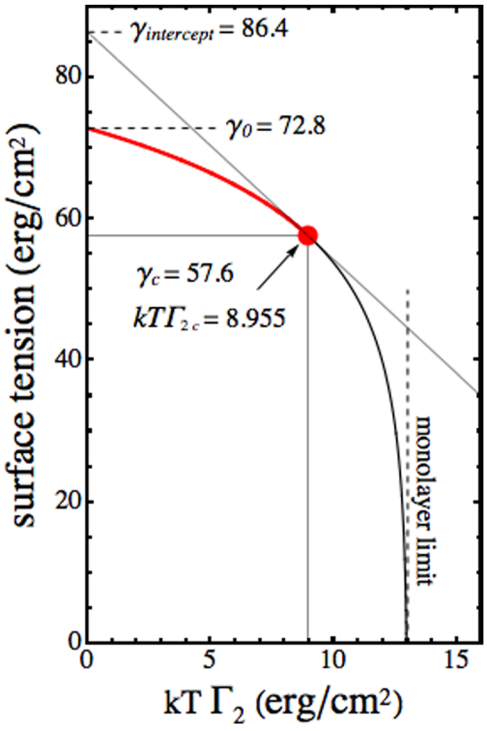

FIG. 2. Combined Szyszkowski–Langmuir plot showing droplet surface tension as a function of superficial density from Eq. (4.8). Black and red regions correspond to the stable and unstable branches of the surfactant Köhler curve, respectively. The red marker indicates the maximum superficial density and minimum surface tension, achievable at the critical droplet size for the indicated monolayer limit, Γ_m. The equality limit of 4.2 is satisfied at this point in the strong surfactant limit. Analytic expressions for γ_c and $kT\Gamma_{2c}$ are available from Eq. (4.10). Because Γ_m is the same for each, this figure applies to all of the compounds within the Meissner and Michaels group.

Interestingly, a fundamental lower limit on surface tension at the Köhler maximum is implied by (4.2) as used in Eq. (4.10). Recalling the condition $\gamma_{int} - \gamma_c = \gamma_c/2$, where γ_{int} is the tangent intercept and γ_c is surface tension at the Köhler maximum, it follows that $\gamma_c \geq 2\gamma_0/3$; otherwise, $\gamma_{int} < \gamma_0$, which is impossible due to the convexity of Eq. (4.8) on which the tangent construction of Fig. 2 is based. Higher superficial densities (lower surface tensions) are

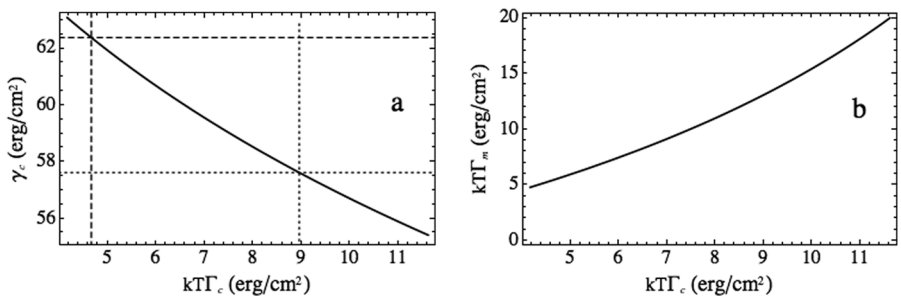

FIG. 3. (a) Effect of varying $kT\Gamma_m$ (which enters the curve parametrically) on critical superficial density $kT\Gamma_c$ and surface tension γ_c at the Köhler maximum. (b) $kT\Gamma_m$ vs $kT\Gamma_c$.

possible for sub-critical droplets along the stable branch of the Köhler curve, lower portion of the curve in Fig. 2, but these are below the activation threshold.

Measurements on a wider set of surfactants that include a number of organic compounds typically found in atmospheric aerosols (see, for example, Fig. 1 of Petters and Petters, 2016) are indicative of significant differences in monolayer superficial density, Γ_m. Figure 3(a) shows surface tension as a function of superficial density at the Köhler maximum. Both quantities depend parametrically on $kT\Gamma_m$, which varies as shown in Fig. 3(b). Dotted crosshairs mark the conditions used in Fig. 2.

Dashed crosshairs are from a fit of the Szyszkowski equation to surface tension measurements on bulk samples of fogwater by Facchini *et al.*, 1999; Facchini *et al.*, 2000, with the corresponding Szyszkowski and combined Szyszkowski–Langmuir curves shown in Fig. 4. In this case, γ_c and $kT\Gamma_c$ take the unique values $\gamma_c = 62.4 erg/cm^2$ and $kT\Gamma_c = 4.66$ at the Köhler maximum. This can be compared with the monolayer value, $kT\Gamma_m = 5.48$, for a critical monolayer coverage fraction for this case of 85% vs 69% found for the compounds of Meissner and Michaels. The dashed curve on the right-hand side of Fig. 4 shows the range of surface tensions measured on bulk fogwater samples—from nearly pure water 72.8 erg/cm^2 to about 50 erg/cm^2, a reduction of about 30%. From γ_c and $kT\Gamma_c$, the saturation ratio and droplet radius at the Köhler maximum are obtained [S_c from Eq. (4.11) and r_c from Eq. (4.12)]. The proportionality $\ln S_c \propto A^{3/2}B^{-1/2} \propto \gamma_c^{3/2}$ implies a reduction in $\ln S_c$ that is less than half the expected value based on the lower range of the bulk measurements. The limited reductions in surface tension achievable at the Köhler maximum are expected to have significant implications for CCN inventories used in models.

Ideal surfactant model: For very dilute solutions that are also ideal (at least for non-electrolytes), the variation of surface tension with solute concentration is linear in superficial density (Adamson and Gast, 2012),

$$\gamma_0 - \gamma = kT\Gamma_2, \tag{4.13}$$

which is a linearization of the Szyszkowski–Langmuir model [Eq. (4.8)]. The Langmuir adsorption isotherm [Eq. (4.7)] is also linearized,

$$\Gamma_2 = \Gamma_m K x_2, \tag{4.14}$$

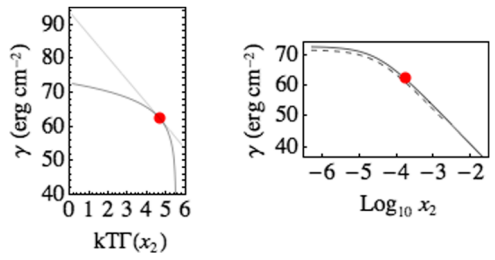

FIG. 4. Combined Szyszkowski–Langmuir (left) and Szyszkowski (right) plots. The right plot is from the empirical fit of bulk surface tension measurements on fogwater samples by Facchini *et al.* (1999). The dashed curve (shifted for clarity) shows the range of surface tensions reported from the bulk samples. The markers show the only conditions possible at the Köhler maximum.

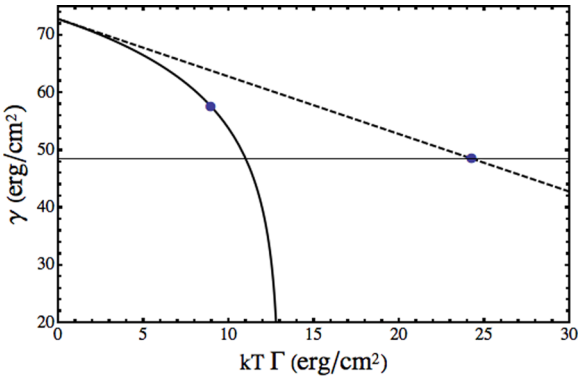

FIG. 5. Comparing the Szyszkowski–Langmuir (solid curve, same as in Fig. 2) and ideal (dashed line) surfactant models. Horizontal line: $\gamma_c = 2\gamma_0/3$. Markers show conditions at the Köhler maximum for the two models. Regions above (below) the markers correspond to unstable (stable) branches of the corresponding Köhler curves. For an ideal surfactant, $\gamma_0 = \gamma_{int}$.

and the pair together satisfy the Gibbs adsorption equation. Substitution into (4.2) at equality gives the conditions at the Köhler maximum $\gamma_c = 2\gamma_0/3$ and $kT\Gamma_c = \gamma_0/3$, implying that the ideal surfactant and bulk limits share the same locus of Köhler maxima. Figure 5 presents a comparison of the models. The line, γ vs $kT\Gamma_2$, is self-tangent in the ideal model with a slope of −1.

V. THE GENERAL CASE OF A PARTITIONED SOLUTE

Inequality (3.10) applies to the general partitioning of a single solute between the surface and the volume of the droplet, with (3.12) and (3.14) obtained as limiting cases considered in Secs. IV B and IV A, respectively. The extra complexity in (3.10) accounts for changes in partition fraction with droplet size in the general case.

Next, we consider two compounds, n-butanol and octanoic acid (OA), from the group of 25 studied by Meissner and Michaels and thus well approximated as having the same superficial density at monolayer coverage (i.e., Fig. 2 applies to both). The partition coefficients, on the other hand, differ significantly with OA showing a much stronger preference for the surface phase.

Method of calculation: The following sequence of steps was employed in the calculations used to produce Figs. 6–9 for general partitioning: Given a value for x_2 in the range of interest, obtain γ from Eq. (4.5) and Γ from Eq. (4.7). The droplet radius is obtained from species conservation, $n_2^b + n_2^s = n_2$, which can be expressed in the form of a cubic equation, $ar^3 + br^2 = n_2$, with $a = 4\pi x_2/3v_1$ and $b = 4\pi\Gamma_2$. The radius is given as the positive real root of the cubic for specified n_2 or r_{dry}. The bulk and surface occupation numbers then follow as $n_2^b = ar^3$ and $n_2^s = br^2$, where r is the root. This suffices for the generation of Figs. 6 and 8. Saturation ratios needed to generate the Köhler curves shown in Figs. 7 and 9 were obtained from the pressure equation [Eq. (4.1)] with $\Delta P = 2\gamma/r$.

n-Butanol: Figure 6 shows an example of partitioning for $K_{but} = 1.27 \times 10^3$, representative of members of the "class 4" compounds

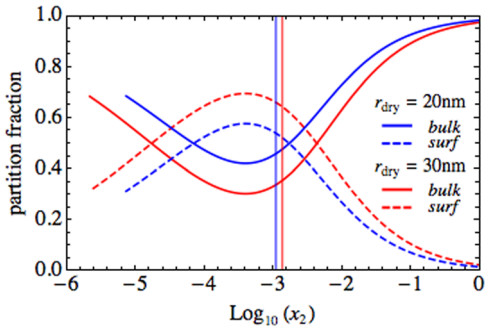

FIG. 6. Solute partitioning for n-butanol showing the fraction of n_2 in bulk (n_2^b/n_2), solid curves and at the surface (n_2^s/n_2) dashed curves. Vertical lines indicate bulk compositions at the critical droplet sizes. Note that the larger value of r_{dry} gives rise to larger critical droplets relatively enriched in bulk and depleted at the surface.

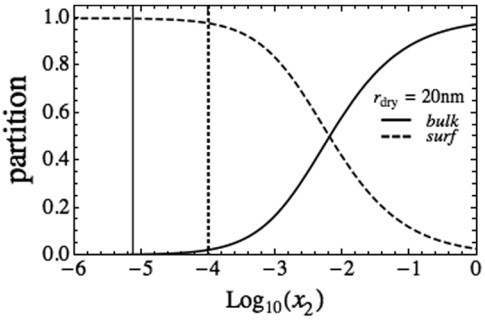

FIG. 8. Solute partitioning for octanoic acid. Solid and dashed curves show partitioned fraction to bulk, n_2^b/n_2, and surface, n_2^s/n_2, respectively. Vertical lines mark solute concentration at the critical drop size (solid), surface partition fraction close to unity, and at the saturation limit (dotted).

of the Meissner–Michaels grouping that includes *n*- and isobutyric acid and *n*- and isobutyl alcohol. The red and blue curves shown in the figure were obtained for two values of r_{dry} (20 nm and 30 nm) and $v_2 = 1.5 \times 10^{-22}$ cm^3 characteristic of butanol in the dry particle. Vertical lines indicate the bulk compositions of the droplets at their respective critical sizes.

Figure 7 shows the locus of Köhler maxima (red curve) for the same butanol partitioning case shown in Fig. 6. Hyperbolic curves are as follows: Kelvin curve for $\gamma = \gamma_{int}$, the intercept value of surface tension in Fig. 2 (dotted); Kelvin curve for water, $\gamma = \gamma_0$ (upper solid curve); locus of Köhler maxima in the surfactant limit (upper dashed curve at 2/3 height of the dotted curve); and locus of Köhler maxima in the bulk limit (lower dashed curve at 2/3 height of the water curve). The partitioned result (red curve) is bounded by the surfactant and bulk limiting dashed curves. Note a clear preference to follow the surfactant (bulk) limiting curve for small (large) values of droplet critical radius. For the special case that $\gamma_{int} = \gamma_0$, as with the ideal surfactant model, the limiting dashed curves coincide, implying that the Köhler maxima for the bulk and surfactant limiting cases share the same locus in that model.

Octanoic acid: Figure 8 shows the partitioning of OA in the SL model. This compound, with partition coefficient $K_{oct} = 2.94 \times 10^5$ (Meissner and Michaels, 1949), has properties close to the surfactant limit at the Köhler maximum. The saturation limit for OA in water, not taken into account in the calculations, is indicated for reference in the figure. The solution is seen to be under-saturated at the Köhler maximum (solid line).

Figure 9 shows Köhler curves for OA together with the locus of surfactant-limit critical points from Eq. (4.11), for comparison, and the Kelvin curve from Eq. (2.2) (dashed and solid hyperbolic curves, respectively). Solid Köhler curves were obtained allowing for general partitioning, as described above. The corresponding dotted curves assume the surfactant limit independent of droplet size. These two distinct models agree at the Köhler maxima, and at larger sizes, but show departure at smaller radii where the bulk solutions are more concentrated and quickly approach saturation. The surfactant effect is stronger than the bulk effect in this sub-critical (stable droplet) regime, as evidenced by the solid curves, which include partitioning, showing less reduction in saturation ratio compared with the dotted curves obtained under the assumption that all of the solute is at the surface. The effect is especially evident for the

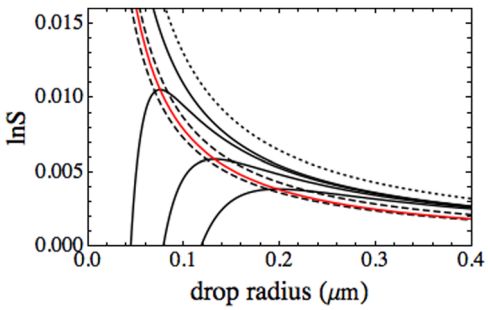

FIG. 7. Locus of Köhler maxima (red) and individual Köhler curves for butanol at equivalent dry radii (top to bottom) of 20 nm, 30 nm, and 40 nm. The three Köhler maxima lie along the red curve. See text for the description of the hyperbolic curves.

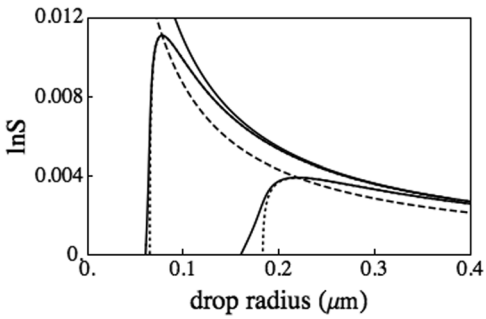

FIG. 9. Köhler curves for OA: $r_{dry} = 20nm$ (upper) and 40 nm (lower) solid curves. Dashed hyperbolic curve: locus of Köhler maxima in the surfactant limit. Solid hyperbolic curve: Kelvin curve for water. See text for explanation of the dotted Köhler curves.

40 nm seed. Nevertheless, for OA, the region around the Köhler maximum is well described by assuming the strong surfactant limit. In this context, it is worth mentioning that the critical solute concentration, indicated by the vertical solid line in Fig. 8, is visibly unchanged on doubling r_{dry} to 40 nm. This is to be expected from the Langmuir adsorption equation as follows: to the extent that Γ_c is constant, x_c will be too. However, Γ_c is constant at the Köhler maximum in the surfactant limit and very nearly constant for OA.

There are several approaches to determining the loci of Köhler maxima. One approach, described in Sec. III, involves equating two expressions for $d\mu_2/dr$: Eq. (3.8), which is valid only at the Köhler maximum, and Eq. (3.9), which is valid at any radius. Solving the resulting equality yields the Köhler maximum. A second approach, dependent only on the total number of molecules of solute present, n_2, irrespective of partitioning, is described in Sec. VII.

VI. MIXTURES

Inequality (3.15) applies to any number of components whether they favor the bulk, surface, or partition between the two. The equality condition

$$\left(r\frac{x_2}{v_1}+2\Gamma_2\right)\frac{d\mu_2}{dr}+\left(r\frac{x_3}{v_1}+2\Gamma_3\right)\frac{d\mu_3}{dr}+\cdots=-\Delta P \tag{6.1}$$

is satisfied at a Köhler extremum for the mixture: The relative amounts of solute species 2, 3, ... reflect the composition of the dry particle seed. In the most general case, these species interact and each derivative would be taken with the chemical potentials of the others held constant, a procedure requiring knowledge of the multicomponent phase diagram. To illustrate (6.1), the problem is simplified first by assuming species independence. In the κ-Köhler formulation, this assumption is in place for the solution phase through the Zdanovskii, Stokes, and Robinson (ZSR) approximation, in which the different amounts of water assigned to each soluble species are assumed additive (Stokes and Robinson, 1966; Petters and Kreidenweis, 2007). At this stage, the problem is solvable using (3.9) for the derivative of the chemical potential of each species with respect to radius in (6.1). A further simplification is to assume strong preference (not uncommon) for each species to partition either to the interior solution or to the droplet surface, at least at those concentrations close to the Köhler maximum, c.f. Fig. 8 for octanoic acid. The result is a straightforward extension of Sec. II to mixtures of water-soluble species and surfactants.

The species independence and strong preference assumptions together reduce the chemical potential derivatives from their fully partitioned form (3.9) to the simpler expressions

$$\frac{d\mu_i}{dr}=-\frac{3kT}{r} \tag{6.2}$$

for species i, present in solution, and

$$\frac{d\mu_j}{dr}=\frac{2kT}{r}\left(\frac{\partial\gamma(r)}{\partial kT\Gamma_j}\right) \tag{6.3}$$

for species j, present at the surface. As with (3.9), Eqs. (6.2) and (6.3) apply at any radius, not just at a Köhler maximum.

Multiplying inequality (6.1) by $-v_1/kT$, inserting Eqs. (6.2) and (6.3), and canceling terms gives at the stability limit

$$\ln S_c=2\sum_i x_i-\frac{2v_1}{kTr_c}\sum_j 2kT\Gamma_j(r_c)\left(\frac{\partial\gamma}{\partial kT\Gamma_j}\right)_{r=r_c}=\frac{2(B_I+B_J)}{r_c^3}, \tag{6.4}$$

where the saturation ratio has entered through ΔP by way of Eq. (4.1) and

$$B_I/r_c^3=\sum_i B_i/r_c^3=\sum_i x_i,$$
$$B_J/r_c^3=\sum_j B_j/r_c^3=-\frac{2v_1}{kTr_c}\sum_j kT\Gamma_j(r_c)\left(\frac{\partial\gamma}{\partial kT\Gamma_j}\right)_{r=r_c}. \tag{6.5}$$

The presence of additional species in the mixture, whether surface active or not, increases critical droplet size, resulting in concomitant lowering of the critical superficial density. Indeed, the critical coordinates $\{\Gamma_j(r_c),\gamma_c\}$ can now lie anywhere along the unstable portion of the Szyszkowski–Langmuir curve (e.g., the red section of the curve in Fig. 2) as the region of stability changes depending on seed particle composition while remaining independent of seed size.

Equations (6.4) may be compared with the GKK form [Eq. (2.5)] extended to a mixture,

$$\ln S(r)=-\sum_i x_i+\frac{v_1}{kT}\Delta P=-\sum_i x_i+\frac{2v_1\gamma}{kTr}. \tag{6.6}$$

Whereas Eq. (6.4), derived from inequality (6.1), applies only at a Köhler extremum, Eq. (6.6) applies at any droplet radius, becoming

$$\ln S_c=\frac{A_c}{r_c}-\frac{B_I}{r_c^3} \tag{6.7}$$

at the Köhler maximum. Equating these two independent expressions at the Köhler maximum gives

$$\frac{A_c}{r_c}=\frac{(3B_I+2B_J)}{r_c^3} \tag{6.8}$$

with $A_c=2v_1\gamma_c/kT$. The critical surface tension and droplet size are available from Eq. (6.8). In particular,

$$r_c^2=\frac{(3B_I+2B_J)}{A_c}. \tag{6.9}$$

The minimum surface tension is obtained in the limiting case that the entire seed is composed of surfactants (i.e., $B_I=0$). Inserting (6.5) into (6.8) gives

$$\gamma_c^S=-2\sum_j kT\Gamma_j(r_c)\left(\frac{\partial\gamma}{\partial kT\Gamma_j}\right)_{r=r_c}, \tag{6.10}$$

where the superscript refers to the surfactant limit. Equation (6.10) is the obvious extension of (3.12) to multiple surfactant species.

The prevalence of hyperbolic curves proportional to the Kelvin curve, either as a locus of Köhler maxima for an internal mixture of seed particles of fixed composition and variable size or as boundaries for a 2D locus of Köhler maxima for mixtures having variable composition and size, is nicely explained from these results: Rewriting Eq. (6.4) as

$$r_c^3 \ln S_c = 2(B_I + B_J)$$

and dividing by Eq. (6.9) gives the general result

$$r_c \ln S_c = \left(\frac{2B_I + 2B_J}{3B_I + 2B_J}\right) A_c. \tag{6.11}$$

This reduces in the absence of surfactant ($B_J = 0$) to

$$r_c \ln S_c = \frac{2}{3} A_c = \frac{2}{3} A_0, \tag{6.12}$$

the universal curve for mixtures containing one or more soluble inorganic compounds. Because, as demonstrated in Sec. IV for the ideal and Szyszkowski–Langmuir surfactant models, the surface tension cannot go below $2\gamma_0/3$, Eq. (6.12) gives a lower bound hyperbola for any mixture described by these models.

In the surfactant limit, Eq. (6.11) reduces to

$$r_c \ln S_c = A_c, \tag{6.13}$$

which is minimized for $A_c = A_c^S = 2\nu_1 \gamma_c^S / kT$ for a mixture of surfactants using Eq. (6.10). For the complete locus of Köhler maxima, in the general case that both particle size and composition vary, Eqs. (6.12) and (6.13) can be combined to obtain

$$\frac{2}{3} A_0 \le r_c \ln S_c \le A_c^S. \tag{6.14}$$

Extension of the κ-Köhler model to include surfactants*:* In Eq. (6.5), the assignment

$$\sum_i x_i = \frac{B_I}{r_c^3} \tag{6.15}$$

was made using $B_I = \kappa_I r_{dry}^3$ from Eq. (2.11), based on the volume-additive property of κ,

$$\kappa_I = \sum_i \frac{r_{dry,i}^3}{r_{dry}^3} \kappa_i \equiv \sum_i \varepsilon_i \kappa_i. \tag{6.16}$$

Summing over water-soluble species i gives $\sum_i \varepsilon_i = \sum_i r_{dry,i}^3 / r_{dry}^3 = r_{dry,I}^3 / r_{dry}^3$ for the fractional volume of water-soluble species in the dry seed particle.

To represent surfactants in a similar fashion, a species- and model-dependent parameter η for the surface-active species is introduced. For species j in the Szyszkowski–Langmuir model,

$$\eta_j = \frac{2}{3}\left(\frac{1}{1 - \frac{\Gamma_j}{\Gamma_{mj}}}\right)\frac{\nu_1}{\nu_j}, \tag{6.17}$$

reducing to

$$\eta_j = \frac{2}{3}\frac{\nu_1}{\nu_j} \tag{6.18}$$

in the ideal case. The additive rule for η is the same as for κ,

$$\eta_J = \sum_j \eta_j \frac{r_{dry,j}^3}{r_{dry,J}^3} \equiv \sum_j \varepsilon_j \eta_j, \tag{6.19}$$

and $B_J = \eta_J r_{dry}^3$ completes the analogy. As the strong-preference approximation assumes that each species is either water-soluble or surfactant, we have $\sum_i \varepsilon_i + \sum_j \varepsilon_j = 1$. As composition is changed, the κ values remain unchanged, as do the η values in the ideal case, while the η values in the S–L model need to be recomputed using Eq. (6.4).

Implementation of the η-Köhler extension is illustrated by showing that the well-known 3/2 power-law scaling between effective dry particle radius and critical wet radius applies as well to mixtures that include both water-soluble species and surfactants,

$$r_c^2 = \frac{(3B_I + 2B_J)}{A_c} = \frac{(3\kappa_I + 2\eta_J)}{A_c} r_{dry}^3. \tag{6.20}$$

Critical droplet concentration, proportional to r_{dry}^3 / r_c^3, continues to increase as $1/r_c$.

Figure 10 shows the locus of Köhler maxima for seed particles consisting of mixtures of NaCl and octanoic acid of varying size and composition. This is indicated by the shaded region bounded by the lower and upper dashed hyperbolic curves for pure NaCl and pure OA (γ_c^S=57.6), respectively. The dotted curve is the specific locus for composition 10% NaCl and 90% OA by number (8.2% NaCl and 91.8% OA by volume). $\kappa_{\mathrm{NaCl}} = 1.25$ is unchanged, while η_{OA} depends on composition, with $\eta_{OA} = 0.17$ for the 10–90 mixture. The red curves (see caption) were obtained with fixed total occupation number $n_2 + n_3 = 1.6 \times 10^5$, corresponding roughly to a 20 nm

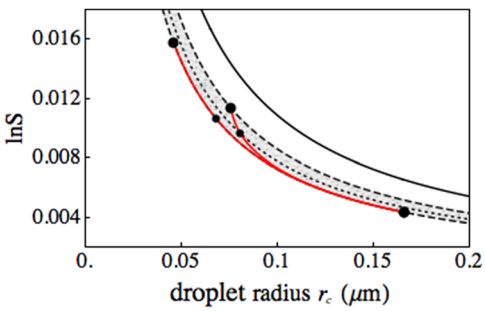

FIG. 10. Loci of Köhler maxima for binary seed particles, ~20 nm in radius, consisting of mixtures of salt and octanoic acid. Composition ranges from pure octanoic acid (upper larger markers) to pure salt (lower merged marker). Upper and lower red curves, Szyszkowski–Langmuir and ideal surfactant models, respectively. Black solid curve, Kelvin relation for pure water. Loci of Köhler maxima for pure octanoic acid, upper dashed curve; pure salt, lower dashed curve; and a 10% salt, 90% octanoic acid mixture, dotted curve. Smaller markers, results from the 10% salt mixture calculation according to the two models.

radius particle for NaCl and a slightly larger one on full replacement of the NaCl ion pairs (component 2) with OA (component 3), keeping the total occupation number constant. Note the merging of the curves computed using the Szyszkowski–Langmuir and ideal models (upper and lower red curves, respectively) as the number of molecules of surfactant and superficial density are reduced on replacement with salt. The figure shows that the initial replacement of OA with even a small amount of salt (0%–10%) results in a significant reduction in the Köhler activation threshold, most notably in the Szyszkowski–Langmuir model. The effect is weaker and in the opposite direction when it is the salt that is initially replaced. Finally, the dashed curves, which are identical to those in Figs. 1 and 9, are seen to bound the locus of Köhler maxima for the mixture [shaded region consistent with inequalities (6.14)].

VII. CONNECTIONS TO CLASSICAL NUCLEATION THEORY

The barrierless Köhler activation process differs fundamentally from nucleation, which requires a thermally driven barrier crossing. During the Köhler process, critical droplets are formed and transformed spontaneously from infinitesimally sub-critical droplets to infinitesimally super-critical ones as the threshold level of water vapor saturation is reached—a barrierless transition. Nevertheless, there are connections between the two processes, as previously explored in the absence of surfactant effects (Reiss and Koper, 1995; Mirabel *et al.*, 2000). Here, we focus on the reversible work of critical droplet formation *directly from the vapor*, W^*, a quantity whose derivative with respect to the chemical potential of species i gives the *total* number of molecules of species i present in the droplet independent of surface-bulk partitioning. The work of critical droplet formation in classical nucleation theory takes the form

$$W^* = -V\Delta P + 4\pi r^2\gamma, \tag{7.1}$$

where V is the droplet volume. Moreover, each of the terms on the right-hand side is individually related to W^*,

$$\begin{aligned} 2W^* &= V\Delta P, \\ 3W^* &= 4\pi r^2\gamma. \end{aligned} \tag{7.2}$$

These relations, also found in Gibbs (1878) (p. 421 of the cited reference), have recently been extended for applications to heterogeneous as well as homogeneous and molecular-based nucleation processes (McGraw *et al.*, 2018). From a cloud physics perspective, W^* would seem to have little bearing on the Köhler problem as critical droplet assembly directly from water vapor and particle seed is not taking place. Nevertheless, W^* retains the theoretical value; it is an especially convenient thermodynamic potential for making sense of the intertwined relationships existing between changes in surface and volume work, between droplet size and seed composition, and between surface tension and Laplace pressure at a Köhler maximum.

Inverting Eq. (3.8) yields an expression for $dr/d\mu_2$,

$$\frac{dr}{d\mu_2} = -\frac{(3n_2^b + 2n_2^s)}{8\pi r\gamma}. \tag{7.3}$$

This is simpler than the reciprocal of (3.9) would imply, but (3.8) is valid only at a Köhler maximum, whereas (3.9) holds for any radius. Converting Eq. (7.3) from the droplet radius to surface area (or volume) results in derivatives of droplet surface area (or volume) with respect to chemical potential,

$$\gamma\frac{d(4\pi r^2)}{d\mu_2} = \Delta P\frac{dV}{d\mu_2} = -(3n_2^b + 2n_2^s). \tag{7.4}$$

Combining Eq. (7.4) with (3.3) and (3.4) gives the change in surface (or volume) work with respect to the change in chemical potential,

$$\frac{d(4\pi r^2\gamma)}{d\mu_2} = \gamma\frac{d(4\pi r^2)}{d\mu_2} + 4\pi r^2\frac{d\gamma}{d\mu_2} = -(3n_2^b + 2n_2^s) - n_2^s = -3n_2, \tag{7.5}$$

$$\frac{d(V\Delta P)}{d\mu_2} = \Delta P\frac{dV}{d\mu_2} + V\frac{d\Delta P}{d\mu_2} = -(3n_2^b + 2n_2^s) + n_2^b = -2n_2. \tag{7.6}$$

Comparing Eqs. (7.5) and (7.6) with the corresponding Gibbs identities for reversible work from Eqs. (7.1) and (7.2) gives in either case

$$\frac{dW^*}{d\mu_2} = -n_2. \tag{7.7}$$

This equation holds for each species present in the droplet (including water). Derivatives are taken holding the chemical potentials of the other species present constant. These "nucleation theorems" give the molecular content of a multicomponent critical nucleus in terms of its reversible work of formation from vapor (Oxtoby and Kashchiev, 1994). Here, we have shown that the theorems apply as well to the incipient multicomponent droplets at the vapor saturation threshold for cloud drop formation.

Figure 11 shows an application of the results of this section to another determination of conditions at a Köhler maximum. This method depends only on the total number of molecules present in the droplet, irrespective of their partitioning. The figure shows reduced surface work as a function of reduced chemical potential. Similar curves for the volume work or total work, W*, would lie at

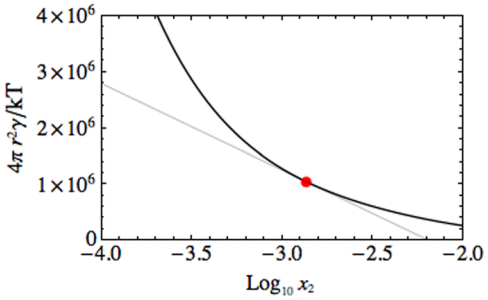

FIG. 11. Tangent construction for the Köhler maximum for a case of general partitioning. Reduced surface work of droplet formation vs reduced chemical potential for butanol at equivalent dry diameter r_{dry} = 20 nm (solid curve). The critical slope is $-3n_2$ from Eq. (7.5), multiplied here by 2.303 for the use of the common log. The marker indicates the unique set of coordinates present at the Köhler maximum.

2/3 height and 1/3 height, respectively, of the surface work curve. The tangent slope of the surface work curve at the Köhler maximum is $-3n_2$ (before correcting for use of the common log) in agreement with Eq. (7.5). Correspondingly reduced, the critical slope for the volume work (if shown) would be $-2n_2$, and for W^*, it would be $-n_2$ in agreement with Eqs. (7.6) and (7.7).

VIII. DISCUSSION AND SUMMARY

An early droplet stability model of Gibbs (Gibbs, 1878) has been developed and used to systematically reformulate the Köhler theory of cloud droplet activation in a way that seamlessly includes water-soluble species and surfactants. The model relies on only the most fundamental principles of chemical thermodynamics, specifically the Gibbs adsorption equation (3.3), its pressure analog (3.4), and conservation of solute species. Even the background phase surrounding the aqueous solution droplet is unspecified—it could be vapor or even ice. There is no restriction placed on the activity of the solute, either within the drop or at its surface, other than the requirement that it has the same value in equilibrium. Gibbs assumed a solute activity proportional to concentration, but this assumption is not required by the model. The only requirement is that the critical droplet radius be large relative to interfacial thickness, as discussed by Gibbs himself and noted in Sec. IV.

The last requirement is well satisfied for typical cloud environments where supersaturations are low, usually less than 1 or at most a few percent. Under these conditions, the nascent critical droplets are sufficiently large that any intrinsic dependence of surface tension on the droplet curvature can be neglected, while the compositional dependence of the surface tension through changes in droplet surface-to-volume ratio and solute partitioning is retained. This last point implies that interfacial models developed to treat flat surfaces (e.g., Dutcher and Wexler, 2013; Wang and Wexler, 2013) remain applicable to the critical droplets at a Köhler maximum.

In its application to Köhler theory, the stability analysis of Gibbs provides a systematic framework that places the treatment of surfactant and solution effects on a more or less equal footing. The new framework inherits the symmetry manifested between (3.14) and (3.12), which constrain how critical supersaturation and solute concentration, and surface tension and superficial density, respectively, vary along loci of Köhler maxima. These two fundamental inequalities serve as the basis for our reformulation of Köhler theory.

A key finding of the present study is that the ability of surfactants to lower surface tension *at a Köhler maximum* is surprisingly limited: for the models tested (Szyszkowski–Langmuir and ideal), the lowering relative to pure water is at most 1/3, and that limit is achieved only in the ideal model. The graphical construction of Fig. 2 provides a simple proof of this result for any convex or linear adsorption isotherm. Different models of surface tension and adsorption may lead to different results regarding weakening of the surfactant effect. The extent to which this occurs is an open question. The fundamental methods of Sec. III can provide a detailed case-by-case analysis, as described for the two models considered in Sec. IV B, and may well lead to more general avenues for development in future research.

Increases in critical droplet radius as well as lowering of surface tension reduce the critical saturation threshold required for activation. The analysis of Sec. IV, extended in Sec. VI to mixtures, accounts quantitatively for both effects. The critical wet radius was found to have the same scaling for mixtures of water-soluble and surface-active species, proportional to the 3/2 power of the equivalent dry seed radius, as previously obtained for the bulk limit (Petters and Kreidenweis, 2007; Lewis, 2008). Loci of Köhler maxima were obtained, ranging from individual hyperbolic curves for mixtures of seeds at fixed composition and variable size to bounded, two-dimensional, regions for mixtures of variable composition and size [inequalities (6.14)]. These loci were found to constrain the location of Köhler maxima in a predictable way that should make comparisons between the new theory, CCN measurements, and atmospheric models both more quantitative and easier to implement than was previously possible using the traditional Köhler framework.

ACKNOWLEDGMENTS

We thank Ernie Lewis for valuable advice and discussion, Theresa Kucinski (DOE SCGSR Fellow at BNL) and Laura Fierce for reading through early sections of this manuscript, and the Atmospheric Systems Research (ASR) Program of the U.S. Department of Energy (Grant No: DE-SC0012704) for financial support.

DATA AVAILABILITY

Data sharing is not applicable to this article as no new data were created or analyzed in this study.

REFERENCES

Adamson, A. W. and Gast, A. P., *Physical Chemistry of Surfaces*, 6th ed. (Wiley, New Delhi, 2012).

Albrecht, B. A., "Aerosols, cloud microphysics, and fractional cloudiness," Science **245**, 1227–1230 (1989).

Bermúdez-Salguero, C. and Gracia-Fadrique, J., "Gibbs excess and the calculation of the absolute surface composition of liquid binary mixtures," J. Phys. Chem. B **119**, 5598–5608 (2015).

Bilde, M. and Svenningsson, B., "CCN activation of slightly soluble organics: The importance of small amounts of inorganic salt and particle phase," Tellus B **56**, 128–134 (2004).

Buff, F., "Some considerations of surface tension," Z. Elektrochem. **56**, 311–313 (1952).

Bzdek, B. R., Reid, J. P., Malila, J. and Prisle, N. L., "The surface tension of surfactant-containing, finite volume droplets," Proc. Natl. Acad. Sci. U. S. A. **117**, 8335–8343 (2020).

Dutcher, C. S. and Wexler, A. S., "Statistical mechanics of multilayer sorption: Surface tension," J. Phys. Chem. Lett. **4**, 1723–1726 (2013).

Facchini, M. C., Mircea, M., Fuzzi, S., and Charlson R. J., "Cloud albedo enhancement by surface-active organic solutes in growing droplets," Nature **401**, 257–259 (1999).

Facchini, M. C., Decesari, S., Mircea, M., Fuzzi, S., and Loglio, G., "Surface tension of atmospheric wet aerosol and cloud/fog droplets in relation to their organic carbon content," Atmos. Environ. **34**, 4853–4857 (2000).

Fan, J. *et al.*, "Substantial convection and precipitation enhancements by ultrafine aerosol particles," Science **359**, 411–418 (2018).

Gibbs, J. W., "On the equilibrium of heterogeneous substances," Trans. CT Acad. **III**, 405–408 (1878).

Köhler, H., "The nucleus in and the growth of hygroscopic droplets," Trans. Faraday Soc. **32**, 1152–1161 (1936).

Koop, T., Luo, B., Tsias, A., and Peter, T., "Water activity as the determinant for homogeneous ice nucleation in aqueous solutions," Nature **406**, 611–614 (2000).

Laaksonen, A., McGraw, R., and Vehkamäki, H., "Liquid drop formalisn and free-energy surfaces in binary homogeneous nucleation theory," J. Chem. Phys. **111**, 2019–2027 (1999).

Lewis, E. R., "An examination of Köhler theory resulting in an accurate expression for the equilibrium radius ratio of a hygroscopic aerosol particle valid up to and including relative humidity 100%," J. Geophys. Res. **113**, D03205, https://doi.org/10.1029/2007JD008590 (2008).

Lin, J. J., Malila, J., and Prisle, N. L., "Cloud droplet activation of organic-salt mixtures predicted from two model treatments of the droplet surface," Environ. Sci.: Processes Impacts **20**, 1611–1629 (2018).

McGraw, R. and Liu, Y., "Kinetic potential and barrier crossing: A model for warm cloud drizzle formation," Phys. Rev. Letts. **90**, 018501 (2003).

McGraw, R. and Liu, Y., "Analytic formulation and parameterization of the kinetic potential theory for drizzle formation," Phys. Rev. E **70**, 031606 (2004).

McGraw, R. L., Winkler, P. M., and Wagner, P. E., "A unifying identity for the work of cluster formation in heterogeneous and homogeneous nucleation theory," J. Chem. Phys. **149**, 084702 (2018).

Meissner, H. P. and Michaels, A. S., "Surface tensions of pure liquids and liquid mixtures," Ind Eng. Chem. **41**, 2782–2787 (1949).

Mirabel, P., Reiss, H., and Bowles, R. K., "A comparison of Köhler activation with nucleation for NaCl–H_2O," J. Chem. Phys. **113**, 8194–8199 (2000).

Ovadnevaite, J., Zuend, A., Laaksonen, A., Sanchez, K. J., Roberts, G., Ceburnis, D., Decesari, S., Rinaldi, M., Hodas, N., Facchini, M. C., Seinfeld, J. H., and O' Dowd, C., "Surface tension prevails over solute effect in organic-influenced cloud droplet activation," Nature **546**, 637–641 (2017).

Oxtoby, D. W. and Kashchiev, D., "A general relation between the nucleation work and the size of the nucleus in multicomponent nucleation," J. Chem. Phys. **100**, 7665–7671 (1994).

Pandis, S. N. and Seinfeld, J. H., *Atmospheric Chemistry and Physics: From Air Pollution to Climate Change* (Wiley, New York, 1998), p. 786.

Petters, M. D. and Kreidenweis, S. M., "A single parameter representation of hygroscopic growth and cloud condensation nucleus activity," Atmos. Chem. Phys. **7**, 1961–1971 (2007).

Petters, S. S. and Petters, M. D., "Surfactant effect on cloud condensation nuclei for two-component internally mixed aerosols," J. Geophys. Res. Atmos. **121**, 1878–1895, https://doi.org/10.1002/2015jd024090 (2016).

Pitzer, K. S., "Thermodynamics of electrolytes. I. Theoretical basis and general equations," J. Phys. Chem. **77**, 268–277 (1973).

Pruppacher, H. R. and Klett, J. D., *Microphysics of Clouds and Precipitation* (Springer, New York, 2010), Chap. 6.

Raatikainen, T. and Laaksonen A., "A simplified treatment of surfactant effects on cloud drop activation," Geosci. Model Dev. **4**, 107–116, https://doi.org/10.5194/gmd-4-107-2011 (2011).

Reiss, H. and Koper G. J. M., "The Kelvin relation: Stability, fluctuation, and factors involved in measurement," J. Phys. Chem. **99**, 7837–7844 (1995).

Rosenfeld *et al.*, "Flood or drought: How do aerosols affect precipitation," Science **321**, 1309–1313 (2008).

Ruehl, C. R., Chuang, P. Y., Nenes, A., Cappa, C. D., Kolesar, K. R., and Goldstein, A. H., "Strong evidence of surface tension reduction in microscopic aqueous droplets," Geophys. Res. Lett. **39**, L23801, https://doi.org/10.1029/2012gl053706 (2012).

Shchekin, A. K. and Rusanov, A. I., "Generalization of the Gibbs–Kelvin–Köhler and Ostwald–Freundlich equations for a liquid film on a soluable nanoparticle," J. Chem. Phys. **129**, 154116 (2008).

Sorjamaa, R., Svenningsson, B., Raatikainen, T., Henning, S., Bilde, M., and Laaksonen A., "The role of surfactants in Köhler theory reconsidered," Atmos. Chem. Phys. **4**, 2107–2117 (2004).

Stokes, R. H. and Robinson, R. A., "Interactions in aqueous nonelectrolyte solutions. I. Solute-solvent equilibria," J. Phys. Chem. **70**, 2126–2131 (1966).

Twomey, S., "The influence of pollution on the shortwave albedo of clouds," J. Atmos. Sci. **34**, 1149–1152 (1977).

Toribio, A. R., Prisle, N. L., and Wexler, A. S., "Statistical mechanics of multilayer sorption: Surface concentration modeling and XPS measurement," J. Phys. Chem. Lett. **9**, 1461–1464 (2018).

Wang, J. and Wexler, A. S., "Adsorption of organic molecules may explain growth of newly nucleated clusters and new particle formation," Geophys. Res. Lett. **40**, 2834–2838, https://doi.org/10.1002/grl.50455 (2013).